Polarization transfer in quasifree $(\vec{p},\vec{n})$ reactions on ^{2}H and ^{3,4}He targets at 197 MeV

D. L. Prout,[1,2] J. Rapaport,[3] M. Palarczyk,[3,4] D. A. Cooper,[5] G. Savopulos,[1] C. Hautala,[3] B. Anderson,[2] A. Baldwin,[2] C. C. Foster,[1] W. Gloeckle,[6] C. D. Goodman,[1] R. Howes,[7] M. S. Islam,[7] B. A. Luther,[8] R. Madey,[2] D. M. Manley,[2] J. Sowinski,[1] E. Sugarbaker,[5] T. N. Taddeucci,[9] I. Van Heerden,[1,*] J. Watson,[2] H. Witała,[10] X. Yang,[3] and W.-M. Zhang[2]

[1]*Indiana University Cyclotron Facility, Bloomington, Indiana 47405*
[2]*Department of Physics, Kent State University, Kent, Ohio 44242*
[3]*Ohio University, Athens, Ohio 45701*
[4]*Henryk Niewodniczański Institute of Nuclear Physics, 31-342 Kraków, Poland*
[5]*The Ohio State University, Columbus, Ohio 43210*
[6]*Ruhr-Universität Bochum, D-44780 Bochum, Germany*
[7]*Ball State University, Muncie, Indiana 47306*
[8]*Concordia College, Moorhead, Minnesota 56562*
[9]*Los Alamos National Laboratory, Los Alamos, New Mexico 87545*
[10]*Institute of Physics, Jagellonian University, PL-30059 Cracow, Poland*

(Received 31 July 2001; published 19 February 2002)

In this paper, we present a complete set of polarization-transfer observables measured at 197 MeV in the quasifree region for $(\vec{p},\vec{n})$ reactions on ^{2}H and ^{3,4}He targets. Data were obtained at laboratory scattering angles of 13°, 24°, 37°, and 48° for the ^{2}H target and at 13° and 37° for the ^{3,4}He targets. The data span an energy-loss range up to 150 MeV, with a corresponding momentum-transfer range $q=0.75$–2.4 fm^{-1}. The polarization-transfer observables are used to calculate the center-of-mass polarization observables. The empirical results for the ^{2}H target are compared to the observables obtained from the free nucleon-nucleon database and with Faddeev-type calculations. No discernible differences are observed in either the values of polarization-transfer observables or in the center-of-mass polarization observables among the three nuclei studied in this paper.

DOI: 10.1103/PhysRevC.65.034611 PACS number(s): 25.40.Kv, 24.70.+s

I. INTRODUCTION

The empirical study of nuclear excitations leading to spin-isospin modes are central to our understanding, and in particular a more quantitative description, of nuclear pion physics. Nuclear responses to a one-pion exchange tend to be unrealistically strong, requiring the introduction of nuclear spin-isospin correlations. In a general discussion of the nuclear spin-isospin response, two basic operators are introduced, ''longitudinal'' and ''transverse,'' indicating the preferred alignment between spin and momentum transfer. The spin-longitudinal operator is able to excite states carrying the quantum numbers of the pion and may be studied with hadronic probes. Transverse excitations, on the other hand, are excited in nuclear magnetic isovector transitions and may be studied both with hadronic and electromagnetic probes [1]. In a more realistic representation, the spin-isospin-dependent residual interaction is represented via the exchange of the pion (π) and rho (ρ) mesons and the nuclear short-range correlation parameter g' in the $\pi+\rho+g'$ model [1]. In this model with a standard value of $g'=0.6$, Alberico *et al.* [2] pointed out that the spin-longitudinal interaction becomes attractive for momentum transfers greater than about 1.0 fm^{-1}, while the spin-transverse interaction remains repulsive. Thus the ratio of the spin-longitudinal to spin-transverse response function should be greater than unity for momentum transfers $q \geqslant 1.0$ fm^{-1}.

In an effort to find empirically this expected enhanced ratio between the spin-longitudinal and spin-transverse response functions, Chen *et al.* [3], and later Taddeucci *et al.* [4], have published results of complete sets of polarization observables for quasifree $(\vec{p},\vec{n})$ reactions on ^{2}H, ^{12}C, and ^{40}Ca at a bombarding energy of 495 MeV and scattering angles of 12.5°, 18°, and 27° ($q=1.2$, 1.7, and 2.5 fm^{-1}). The ratio of the evaluated spin responses in an energy-loss range 30–200 MeV is close to 1.0 in contradiction with the expected enhancement. However, a comparison of the separate responses to theoretical calculations seems to reveal a strong enhancement in the spin-transverse channel. This excess strength may mask the effect of pionic correlations in the ratio between the spin response functions. The theoretical results [5] are based on distorted wave impulse approximation (DWIA) with random-phase approximation (RPA) calculations using phenomenological interactions and the $\pi+\rho+g'$ model of the isovector residual particle-hole interaction.

More recently, Wakasa *et al.* [6] published a complete set of polarization-transfer coefficients measured for quasielastic $(\vec{p},\vec{n})$ reactions on ^{2}H, ^{6}Li, ^{12}C, ^{40}Ca, and ^{208}Pb at a bombarding energy of 346 MeV and a laboratory scattering angle of 22° ($q \approx 1.7$ fm^{-1}). The authors used a plane-wave impulse approximation with eikonal and optimal factorization

*Permanent address: University of the Western Cape, South Africa.

approximations to calculate the ratio of spin responses. As was the case at 495 MeV with Taddeucci's data [4], no nuclear medium enhancement of the ratio of the responses was observed. Although the observed spin-longitudinal response is consistent with the pionic enhanced RPA calculations, a large excess for the spin-transverse response is found in comparison with either RPA calculations or spin-transverse responses obtained from electron scattering data.

In a recent paper, Kawahigashi *et al.* [7] present a DWIA formalism for analyzing spin observables excited in charge-exchange reactions leading to the continuum. It utilizes response functions calculated by the continuum RPA, which include the effective mass, the spreading widths, and the Δ degrees of freedom. The nuclear Fermi motion is treated by the optimal factorization, and the nonlocality of the nucleon-nucleon (NN) t matrix by an averaged reaction plane approximation. The calculations of the spin-longitudinal cross sections of ^{12}C, ^{40}Ca$(\vec{p},\vec{n})$ at 495 and 346 MeV [4,6] reasonably reproduced the measured values, however, the calculated spin-transverse cross sections are much smaller than the observed ones. This is consistent with the predicted enhancement of the spin-longitudinal response function R_L. However, the observed spin-transverse cross sections are much larger than the calculated ones, which is not consistent with the predicted quenching of the spin-transverse response function.

Pandharipande and collaborators [8,9] have calculated isovector spin responses of deuterium and integral properties of these responses in light nuclei and nuclear matter from realistic models of nuclear forces. Their results confirm the previous RPA calculations done for heavier nuclei in which the nuclear spin-longitudinal response has more strength than the spin-transverse response. However, the authors question the energy distribution of the strength predicted by RPA and suggest that $(\vec{p},\vec{n})$ polarization-transfer measurements be carried out on light nuclei such as ^{2}H, ^{3}He, and ^{4}He because (a) distortion of the proton and neutron waves will be smaller in these light nuclei, (b) the value of the spin-transverse response can be compared directly with empirical data obtained with electromagnetic probes, (c) the spin response values for the deuteron can be calculated exactly, and (d) medium effects proposed to explain the lack of empirical enhancement of the longitudinal response in ^{12}C and ^{40}Ca presumably should be negligible in these light nuclei.

Koltun [10] has also questioned the energy dependence of the nuclear spin responses, which differs for theories with strong NN nuclear correlations and those from RPA predictions. His results lead to a much reduced sensitivity of nuclear reactions to the correlations that are responsible for pion excess, pointing out that in $(\vec{p},\vec{n})$ spin-transfer data, the expected effects are found to be smaller than the experimental uncertainties.

The empirical observables are the polarization transfer observables D_{ij} (see Sec. IV) and a linear combination of these are used to obtain the polarization observables D_i (see Sec. VI C). The latter may be used to obtain the partial spin-longitudinal and spin-transverse cross sections. With some approximations [11], the empirical spin responses may be obtained from these partial cross sections. Although previous authors [4,6] have compared their results with theoretical models at the level of the spin responses, recently [7] the comparison has been made at the level of partial cross sections because it does not involve the approximations used to obtain the spin responses. In this paper, we choose to compare the empirical D_{ij} values for the ^{2}H$(\vec{p},\vec{n})$ reaction with *ab initio* calculations. The incident proton energy is in the range where ''exact calculations'' for the ^{2}H target may be performed, using the Faddeev method with realistic NN forces.

We have measured a complete set of polarization-transfer data for quasielastic $(\vec{p},\vec{n})$ reactions at 197 MeV on light nuclei targets, ^{2}H and ^{3,4}He, as well as on heavier targets ^{12}C, ^{40}Ca, and ^{208}Pb at momentum transfers, q, between 0.75 and 2.4 fm^{-1} measured at 197 MeV.

The results of this work, together with those for ^{2}H at 346 MeV from Osaka [6] and those obtained at Los Alamos National Lab at 495 MeV [4], represent a rather complete study of the quasielastic region at similar momentum transfers, but at different bombarding energies. They span a region with changes in the distortions of the nuclear mean field and where the free NN t-matrix components are significantly different, allowing for the study of their separation from the underlying nuclear pion physics of interest.

II. EXPERIMENTAL METHODS

The measurements were performed at the Indiana University Cyclotron Facility (IUCF) using the beam swinger, the INPOL neutron time-of-flight facility [12], and the Kent State ''2π'' neutron polarimeter [13]. The experiment was performed during several running time periods that span about 3 yr. Detailed descriptions of the INPOL facility and the neutron polarimeter systems can be found in Refs. [12,13]. Here we present only salient details of the experimental setup relevant to the present experiment.

A. Targets

A complete set of polarization-transfer coefficients was measured for $(\vec{p},\vec{n})$ reactions on self-supported 98% isotopically enriched CD_2 targets with a total thickness of 150 mg/cm^2, and on C targets of the same thickness. The beam intensity was limited to 150 nA with the solid CD_2 target to avoid loss of material. These targets were made of three layers of about 50 mg/cm^2, each covered with 30 μg/cm^2 of Au per side, to disperse the heat generated by the beam energy loss. In a later experiment, a gaseous target was used. The gas target [14] was a stainless steel box, with front and back windows made from a 25.4 μm-thick Havar foil. The absolute cell pressure was as high as 10 atm and the box was cooled down by continuous flow from a LN_2 reservoir. The gas target was mounted in the regular target ladder, enabling the use of either a solid target or a gas target, depending on the experimental demand. Gas full and empty spectra were collected, as well as spectra from a Havar foil three times the thickness of the Havar foil in the gas target windows. We found no difference between the spectra from the empty gas target and from the Havar foil target. This led

us to the conclusion that there was neither significant beam halo striking the cell body nor contaminants buildup on the cold gas cell window. We used the Havar foil spectra as background spectra because with three times shorter runs we obtained the same luminosity. The same gas target was used for all three gases ^{2}H and ^{3,4}He.

B. Polarized proton beam

The High Intensity Polarized Ion Source (HIPIOS) [15] was used to provide up to 78% polarized proton beams with intensities up to 350 nA. The beam polarization was cycled between ''normal'' and ''reverse'' at 30 sec intervals. Superconducting solenoids located in the proton beam line were used to precess the proton spin polarization so as to have on target either of the three spin states normal $\hat{N}$, sideways $\hat{S}$, or longitudinal $\hat{L}$. The settings on the solenoids take into account the proton spin precession caused by the swinger magnets. Values of the proton beam polarization were continuously measured with beam line polarimeters located immediately after the superconducting solenoids [16].

C. Neutron beam line

Magnets located after the scattering target were used to precess the neutron spin into desirable orientations for the measurements of the 3 components of the spin vector. In particular, superconducting solenoids were used to rotate the neutron spin both $+90°$ and $-90°$ about the momentum axis in separate series of runs to correct for possible geometrical asymmetries in the polarimeter. In another series of runs dipole magnets were used to precess the longitudinal component of the neutron spin to a direction normal to its momentum and thus observable in the polarimeter.

Two large-volume neutron polarimeters were used. INPOL was located in the $0°$ neutron beam line and data were acquired at $\theta=0°$, $13°$, and $24°$, while the Kent State University (KSU) 2π polarimeter was placed in the $24°$ neutron beam line to obtain data at $\theta=24°$, $37°$, and $48°$. Data were taken at the common angle $24°$ with both polarimeters to cross check the polarization results. We briefly describe these polarimeters in the next sections, while more detailed descriptions are given in Refs. [12,13] respectively.

D. INPOL polarimeter

INPOL [12] consists of two pairs of detector ''planes'' all oriented perpendicular to the incident neutron flux. Each 1 m^2 ''plane'' consists of ten scintillators that are each 10-cm high, 10-cm thick, and 1-m long. The first three of these planes are stainless steel tanks filled with Bicron BC-517S liquid scintillator, which was chosen for its high hydrogen content (H:C=1.7). The scintillator for the fourth plane, which was added later, is BC-408 plastic and also consists of 10 separate detectors. The front pair of scintillator planes serve as the analyzer of the polarimeter, scattering the neutron such that it is detected in the rear of planes. Time, position, and pulse-height information from both pairs of planes are used to select events where the detected neutron is close to free np scattering kinematics at forward angles, and the resulting analyzing power is enhanced and reproducible. The effective analyzing power for the polarimeter ranged from 0.24 to 0.29 [12]. Both horizontal and vertical scattering were detected allowing for the simultaneous measurements of vertical and horizontal polarization components respectively. Thin plastic scintillators in front of these planes are used to tag charged particles. An intrinsic time resolution of about 300 ps (FWHM) and a position resolution of about 4.5 cm (FWHM) were usually obtained. The neutron flight path to the first detector plane was measured to be 159 m.

E. KSU 2π polarimeter

The KSU 2π polarimeter [13] consists of four 10-cm high, 10-cm wide, and 50-cm long BC-404 plastic scintillators, which are used as neutron scatterers or analyzers. These are situated with the long axis along the neutron's direction of motion. Displaced 160 cm downstream from the center of the front four scintillators is an azimuthally symmetric ''ring'' of 12 large BC-400 plastic scintillation detectors of dimensions 10-cm high by 25-cm wide and 1-m long. The back ''ring'' has a diameter of 116 cm. The scattering angle between the center of the analyzer detectors and the center of any of the ring detectors is $20°$.

Neutrons scattered from the analyzers are detected in this complete azimuthal coverage (catchers). All 16 detectors are mean timed, using fast photomultiplier tubes on each end of the scintillators. Time, position, and pulse-height information from the central and cylindrical detectors were again used to define np scattering kinematics for forward angle neutrons. The effective analyzing power for the polarimeter ranged from 0.38 to 0.40 [13]. An intrinsic time resolution of about 120 ps (FWHM) and a position resolution of about 1.7 cm (FWHM) were obtained. The neutron flight path to the analyzer was set to either about 25 m or 50 m depending on the energy resolution required for the experiment.

F. Polarimeter cross calibrations

In a separate run using the beam swinger INPOL was set at a scattering angle of $24°$, and polarization data were taken for the $^{6}\mathrm{Li}(\vec{p},\vec{n})^{6}\mathrm{Be}$ reaction. The KSU 2π polarimeter was subsequently set at the same scattering angle. The cross section and polarization data were compared over the large energy range of the quasielastic peak and the polarimeters produced consistent results. In general they agree better than 10%.

Neutron energies were measured by time-of-flight from the target to the front detectors, with an overall energy resolution that depended on target thickness. For either polarimeter an energy resolution better than 1.5 MeV (FWHM) was achieved. For INPOL, absolute differential cross sections were obtained using the method described in Ref. [12]. Briefly, the product of the neutron detector efficiency for double scattering and the neutron absorption in air and other material over the 159 m neutron flight path was measured at $0°$ using the $^{7}\mathrm{Li}(p,n)^{7}\mathrm{Be}$ reaction under similar experimental conditions as used for the targets in this study. The $0°$ differential cross section for this reaction is well known from activation measurements [17]. For the KSU 2π polarimeter,

absolute differential cross sections were determined by comparing cross section data obtained at 24° for the ^{7}Li$(p,n)^{7}$Be reaction and for the ^{12}C$(p,n)^{12}$N reaction with previous absolute cross section measurements of these reactions [18,19].

III. DATA REPLAY

The data taken during the experiments were stored on magnetic tapes, which were processed offline. The replay was conducted at several universities and some of the same data were replayed at least by two different groups. These experiments were done at IUCF, two or three times a year in periods of 2–3 weeks, over about 3 yr. It was important to make sure that the several detector's calibrations were the same and that replay software conditions were identical.

The detector's performance was checked at INPOL using data acquired from cosmic rays. An event that required a tenfold coincidence for all the ten cells in a plane indicated the passage of high-energy cosmic-ray muons depositing a known amount of energy in the cell. This type of event was recorded simultaneously with the reaction data being studied. In replay these data were used to calibrate the detectors in pulse height, position of the events, and timing. A fourfold coincidence of signals in all four planes represented cosmic-ray events traversing INPOL in an horizontal direction. These signals, taken without beam, were used to perform a time calibration for the four planes. A more detailed description of the procedure and software used for the calibration may be found in Refs. [20–22].

Because of the geometry of the 2π polarimeter, cosmic rays could not be used to calibrate the device. To monitor the gain of the photomultipliers, light emitting diodes (LEDs) embedded in the light guides of the detectors were pulsed periodically. Drifts in the gain were then corrected by adjusting the high voltage applied to the photomultiplier tubes. The timing of the front four detectors could be monitored by observing the position of gamma-ray events produced when the beam struck the target. These events appear as a narrow peak in a time-of-flight spectrum; changes in the peak position indicate timing drifts and are compensated for during replay of the data. Timing drifts in the back 12 detectors were monitored by observing γ rays generated in the front detectors and detected in the back scintillators. These scattered γ events were produced by both Compton scattering of γ rays generated in the target and by interaction of the neutrons with the carbon in the scintillator. These events did not deposit much energy in either the front or back detectors compared to the primary neutron events, and were isolated by placing low pulse-height gates on the data during the first replay of the data.

IV. DATA REDUCTION

The polarization-transfer coefficients $D_{ij}(i=S',N',L',j=S,N,L)$ relate the outgoing neutron polarization to the incident proton polarization according to the following equation [3]:

$$\begin{pmatrix} p'_{S'} \\ p'_{N'} \\ p'_{L'} \end{pmatrix} = \left[\begin{pmatrix} D_{S'S} & 0 & D_{S'L} \\ 0 & D_{N'N} & 0 \\ D_{L'S} & 0 & D_{L'L} \end{pmatrix} \begin{pmatrix} p_S \\ p_N \\ p_L \end{pmatrix} + \begin{pmatrix} 0 \\ P \\ 0 \end{pmatrix} \right] \times \frac{1}{1+p_N A_y}, \quad (1)$$

where $\vec{p}(p_S,p_N,p_L)$ represents the incident proton polarization and $\vec{p'}(p'_{S'},p'_{N'},p'_{L'})$ indicates the outgoing neutron polarization. The directions of the coordinate system are defined in terms of the incident proton momentum $\vec{k}_{\rm lab}$ and the outgoing neutron momentum $\vec{k'}_{\rm lab}$ in the laboratory frame of reference as $\hat{\mathbf{L}}=\hat{\mathbf{k}}_{\rm lab}$, $\hat{\mathbf{L}}'=\hat{\mathbf{k}}'_{\rm lab}$, $\hat{\mathbf{N}}=\hat{\mathbf{N}}'=(\hat{\mathbf{k}}_{\rm lab}\times\hat{\mathbf{k}}'_{\rm lab})/|\hat{\mathbf{k}}_{\rm lab}\times\hat{\mathbf{k}}'_{\rm lab}|$, $\hat{\mathbf{S}}=\hat{\mathbf{N}}\times\hat{\mathbf{L}}$, and $\hat{\mathbf{S}}'=\hat{\mathbf{N}}'\times\hat{\mathbf{L}}'$.

The incident proton beam was tuned so as to have a polarization with a single dominant component on target. The beam polarization was continuously monitored and this goal was usually achieved; however, if the beam polarization had components other than the one selected (to a level higher than 5%), then the beam was stopped and retuned. Values for the analyzing power A_y, the induced polarization P, and the transfer coefficient $D_{N'N}$ were obtained from results with normally polarized proton beam. The in-plane observables $D_{S'S}$, $D_{L'S}$ and $D_{L'L}$, $D_{S'L}$ are calculated using results obtained with sideways and longitudinal polarized proton beam, respectively. In what follows, we will use the notation D_{ij} without the primes to denote polarization-transfer coefficients, where i represents the outgoing nucleon and j the incident nucleon.

V. EXPERIMENTAL RESULTS

All tabulated results have been transmitted to the National Nuclear Data Center, at Brookhaven National Lab. where they can be retrieved from their CSISRS database at URL www.nndc.bnl.gov.

A. Observables for the ^{2}H$(\vec{p},\vec{n})$ reaction

Observables for the ^{2}H$(\vec{p},\vec{n})$ reaction were obtained at laboratory scattering angles of 13°, 24°, 37°, and 48° from a cross-section-weighted subtraction of the C observables from the CD_2 observables. Data were also obtained at scattering angles of 13° and 37° using a gaseous ^{2}H target with a thickness of 18.1 mg/cm^2. In the latter case, a subtraction was done from an empty gas cell or from data obtained with a Havar foil target three times the thickness of the Havar used in the windows for the gas cell. It was rewarding to observe excellent agreement in the results obtained at the same angles. Preliminary results obtained with the solid targets have been reported by Cooper [20].

We present in Fig. 1 data taken at $\theta_{\rm lab}=13°$. The top panel shows spectra taken with the gaseous cell. The hatched spectrum corresponds to the empty gas cell. The middle panel shows spectra for the CD_2 target and the C "background" spectrum. The bottom panel compares the ^{2}H(p,n) double differential cross section obtained with both targets.

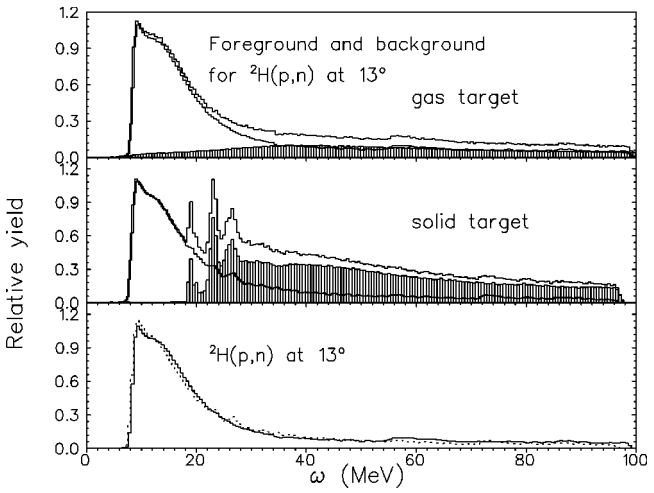

FIG. 1. Foreground and background spectra obtained for the ^{2}H(p,n) reaction at 13°. The top panel represents data obtained using a gas cell with ^{2}H gas. The background from a havar target, is shown with hatched lines. The middle panel indicates data obtained with a solid CD_2 target and the background from a C target. The bottom panel shows a comparison for the double differential ^{2}H(p,n) cross section obtained with the gas target (solid histogram) and the solid target (dotted histogram).

The results indicate agreement well within 10% uncertainty. In general the background provided by the Havar foil is a smooth continuum, while that of the C foil is characterized by the Gamow-Teller transition to the ^{12}N(g.s.), and the low-lying strong dipole and spin-dipole transitions. At higher angles these transitions are weaker.

For the solid targets, absolute double differential cross sections were obtained from the CD_2 and C values according to [3,20]

$$\sigma_{^2\mathrm{H}} = (\sigma_{\mathrm{CD}_2} - \sigma_{\mathrm{C}})/2. \tag{2}$$

Similarly, polarization observables were obtained from

$$D_{^2\mathrm{H}} = (D_{\mathrm{CD}_2} - f_{\mathrm{C}} D_{\mathrm{C}})/(1 - f_{\mathrm{C}}), \tag{3}$$

where D represents one of the observables D_{ij}, P, or A and $f_{\mathrm{C}} = \sigma_{\mathrm{C}}(\omega)/\sigma_{\mathrm{CD}_2}(\omega)$ is the carbon fraction of the CD_2 cross section for energy loss ω. The carbon fraction was estimated based on nominal target thicknesses and integrated beam currents. Relative normalizations were adjusted to obtain the best subtraction of the prominent peak corresponding to the transition to the 4^- state at $E_x = 4.2$ MeV in ^{12}N. For the ^{2}H gas target, similar equations were used, replacing the symbol C for that of Havar. The final values reported in this paper at 13° and 37° correspond to weighted average values from these two targets. The values at 24° and 48° were obtained with only the solid targets. A 3% systematic uncertainty in the background fraction (either C or Havar) has been included in the calculation of the ^{2}H$(\vec{p},\vec{n})$ observables. This uncertainty was estimated from uncertainties in beam current normalizations.

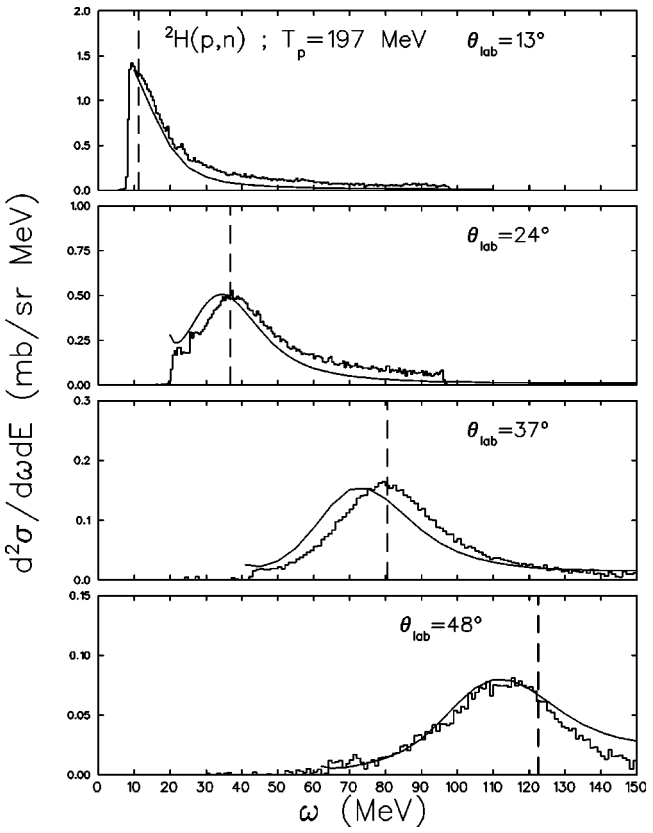

FIG. 2. Laboratory double differential cross section for the ^{2}H(p,n) reaction measured at $E_p = 197$ MeV and scattering angles $\theta_{\mathrm{lab}} = 13°$, 24°, 37°, and 48° as a function of energy loss ω. The vertical dashed lines correspond to the energy loss for free np scattering. The solid line is a result of Faddeev calculations based on the CD Bonn NN interaction.

1. Double differential cross sections for the ^{2}H$(\vec{p},\vec{n})$ reaction

In Fig. 2, we present the ^{2}H$(\vec{p},\vec{n})$ laboratory double differential cross sections measured at $\theta_{\mathrm{lab}} = 13°$, 24°, 37°, and 48°. An uncertainty of $\approx 10\%$ is estimated on the absolute cross section values. In all cases the solid curves represent results from Faddeev-type calculations, see Sec. VI B. The dashed vertical lines mark the energy loss for free np scattering. The top frame of Fig. 2 corresponds to data taken at $\theta_{\mathrm{lab}} = 13°$ ($q \approx 0.73$ fm^{-1}). The peak at lower energy loss, $\omega \approx 9$ MeV, than the dashed vertical line for free np scattering, corresponds to the two-proton final state interaction of the ^{2}H$(p,n)^2$He reaction. At small momentum transfers, this reaction has a $1^+ \rightarrow 0^+$ spin structure. Thus, it can produce observables quite different from those of free np scattering. We have not included this region in our analysis for D_{ij} coefficients. At other angles, the final-state-interaction peak is weaker compared to the quasifree peak.

It is worth noting in Fig. 2 a few points of interest. The Faddeev calculations displayed at $\theta_{\mathrm{lab}} = 24°$ and 37° show the peak of the double differential cross section below the observed peak and below the energy loss for free np scattering. This is a pure kinematics effect resulting for not using relativistic kinematics in the Faddeev calculations. This effect is angle dependent as observed in the figure. Only at

TABLE I. Parameters for the ^{2}H(p,n) quasifree cross sections at 197 MeV. The integrated cross sections correspond to a 70-MeV wide region of excitation starting from threshold at $\theta_{lab}=13°$ and 24°, and centered around the quasifree peak for the other angles. The free *NN* charge-exchange cross sections using the CD Bonn potential are also indicated. An estimated uncertainty of 10% is assigned to the measured values.

θ_{lab}	Peak location ω(MeV)		Integrated σ mb/sr		
	measured	free	σ(measured)	σ(free)	σ(Faddeev)
13°		11.2	22.3	28	16.1
24°	38	36.7	15.7	16.6	14.0
37°	80	80.5	6.5	7.4	5.7
48°	114	122.5	2.6	4.8	3.5

$\theta_{lab}=48°$, the peak of the empirical data is located at an energy loss below that for free *np* scattering. A similar effect has been reported in (p,n) reactions in other nuclei [19], studied at 186 MeV. We do not know the exact reasons for this effect, although it is possible that the neutron efficiency of the KSU "2π" polarimeter is not well understood for low energy neutrons.

We have summed the double differential cross section in the laboratory frame for the ^{2}H(p,n) reaction in a 70-MeV wide region starting from threshold at 13° and 24° and centered around the quasifree peak for the other two angles. The results are compared in Table I with similar sums obtained for free scattering and from the Faddeev calculations. At 13° the quasifree peak has not yet completely developed and the energy resolution of the present experiment is not good enough to separate it from the peak due to the two-proton final-state interaction. Thus the empirical sum contains contributions of a partially blocked quasifree cross section and of the two-proton final-state interaction. At the other three angles, the measured cross section, the value for the free cross section, and the results for the Faddeev calculations compare well with each other. This provides a valuable check on the cross section normalizations used in this experiment.

2. Polarization-transfer coefficients for the ^{2}H$(\vec{p},\vec{n})$ reaction

Values for all D_{ij}, A_y, and P for the ^{2}H$(\vec{p},\vec{n})$ reaction measured at $\theta_{lab}=13°$, 24°, 37°, and 48° are presented in Figs. 3–6, respectively. In all cases the dotted vertical lines mark the energy loss for free *np* scattering. The solid curves correspond to Faddeev calculations, see Sec. VI B. In the top right frame of each figure, values for A_y and P are presented. The latter observable has been offset by 3 MeV in energy loss, in order to visualize them properly. The data presented in these figures are binned in 10 or 15 MeV intervals depending on the statistics achieved at each angle. The statistics are best around the peak of the quasifree scattering cross section, which is the region with the largest double differential cross section. In this region typical uncertainties for the D_{ij} coefficients are about ± 0.05.

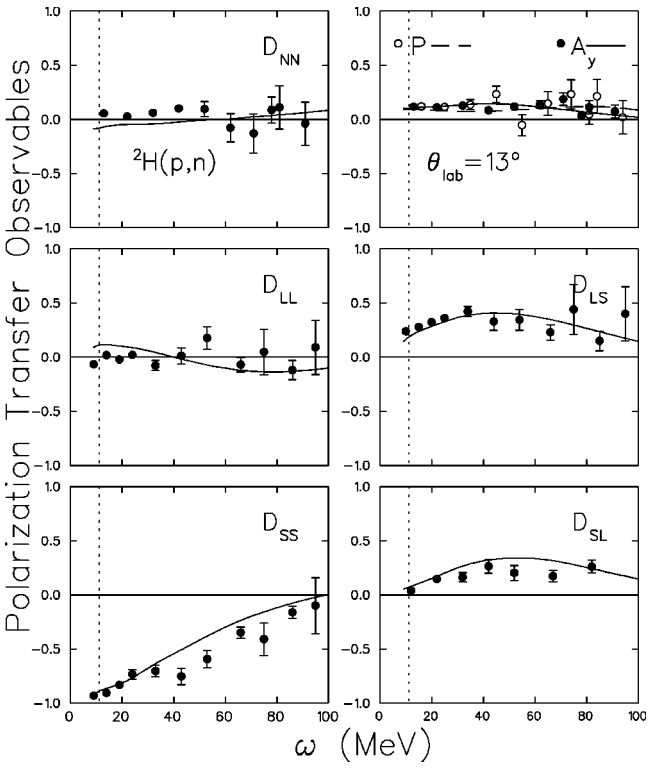

FIG. 3. Polarization-transfer coefficients, analyzing power, and induced polarization for the reaction ^{2}H$(\vec{p},\vec{n})$ measured at $E_p=197$ MeV and at $\theta_{lab}=13°$, $q\approx 0.8$ fm^{-1}. The vertical dashed lines correspond to the energy loss for free *np* scattering. The solid line is a result of Faddeev calculations based on the CD Bonn *NN* interaction.

In general there is good agreement between data and the Faddeev calculations. However, there are two notable discrepancies. One is noted in Fig. 5 where at $\theta_{lab}=37°$ the empirical D_{SS} values are less negative than the calculated ones. The other one is in Fig. 6 where the Faddeev A_y values are not the same as the P values around the quasielastic peak location as it is the case for the other angles. The equality $A_y=P$ around the quasielastic peak is correct only for two body processes as in free *np* scattering. In case of three body processes this is not true and thus existing equalities are only approximate. We do not know the reasons for the discrepancy observed in the D_{SS} values. In cases where other than two-body processes are important, the Faddeev values are different from the *NN* optimal values and in general the agreements are only approximate ones.

B. Observables for the ^{3,4}He$(\vec{p},\vec{n})$ reactions

Observables for the ^{3,4}He$(\vec{p},\vec{n})$ reaction were obtained at laboratory scattering angles of 13° and 37° using a high-pressure, low-temperature gas target. The gas cell temperature and pressure were continuously monitored during the experiments. The thicknesses of the ^{3}He and ^{4}He targets under the above conditions were ≈ 16 mg/cm^2 and ≈ 24 mg/cm^2, respectively. Data were also measured with $^{13}CH_4$ gas in the target cell. This was done at room temperature and at a pressure of ≈ 4 atm. The results, corrected for

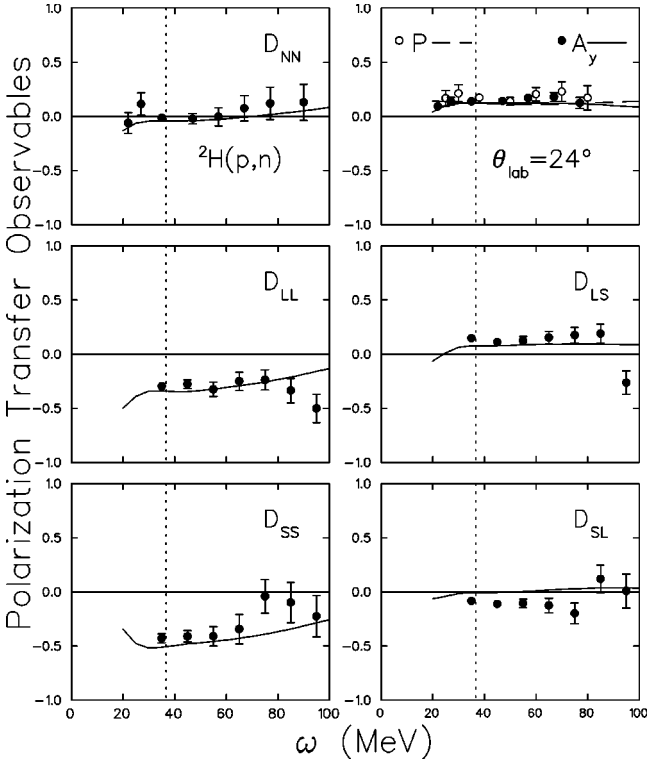

FIG. 4. Same as Fig. 3 but at $\theta_{\rm lab}=24°$, $q\approx 1.4$ fm^{-1}.

target thickness, agreed to within the systematic uncertainties associated with the areal density of the gaseous target ($\approx 5\%$). This gave us confidence that the performance of the gaseous targets was well understood. Data were taken in

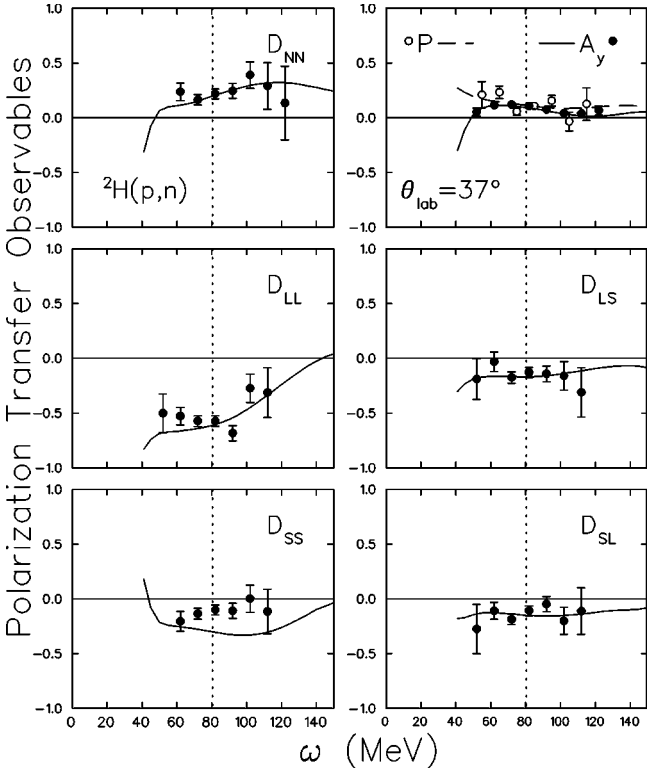

FIG. 5. Same as Fig. 3 but at $\theta_{\rm lab}=37°$, $q\approx 2.0$ fm^{-1}.

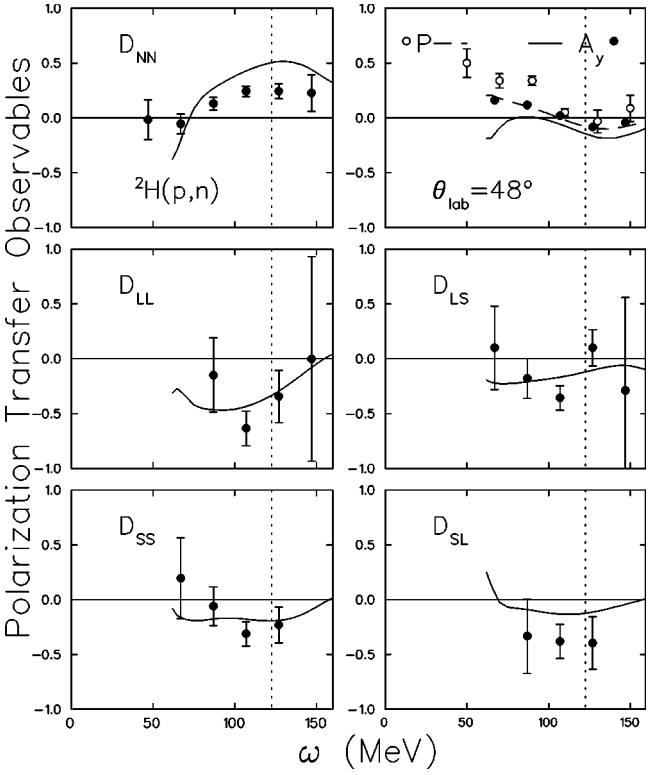

FIG. 6. Same as Fig. 3 but at $\theta_{\rm lab}=48°$, $q\approx 2.4$ fm^{-1}.

1996 and in 1998 for the ^{3}He target. In the second run, the neutron polarimeter located at $\theta=37°$ was moved closer to the target to increase the counting rate. Results for the 1996 run were reported by Savopulos [21]. Excellent agreement was obtained for both runs, and the average results are presented here. Data for ^{4}He were taken during August 1997 and March 1998.

1. Double differential cross sections for the ^{3,4}He$(\vec{p},\vec{n})$ reactions

In Fig. 7 we present laboratory double differential cross sections for the $(\vec{p},\vec{n})$ reactions observed at $\theta_{\rm lab}=13°$ and at $E_p=197$ MeV on the three targets ^{2}H and ^{3,4}He. An uncertainty of $\approx 10\%$ is estimated on the absolute cross section values. The dashed vertical lines represent the location of the energy loss for free np scattering. At this angle the quasielastic peak has not yet completely developed, but based on the shape of the double differential cross section, it seems that the quasielastic peak is more Pauli blocked in ^{4}He than in ^{3}He. In Table II, we present for the three gaseous targets, cross sections summed up in a 70-MeV wide region of excitation starting from threshold at $\theta_{\rm lab}=13°$ ($q\approx 0.9$ fm^{-1}) and centered around the quasifree peak at 37° ($q\approx 2.0$ fm^{-1}) . The free NN charge exchange cross section using the CD Bonn potential is also tabulated.

Palarczyk *et al.* [23] have reported on cross section and analyzing powers for $(\vec{p},n)$ reactions on ^{3,4}He at 200 MeV for angles between $\theta_{\rm lab}=0°$ and 44°. The present results for double differential cross sections and analyzing powers agree well with those reported in Ref. [23]. As pointed out in that reference, the differential cross section for ^{3}He$(\vec{p},\vec{n})$ is expected to be a factor of 2 smaller than the ^{4}He$(\vec{p},\vec{n})$ because

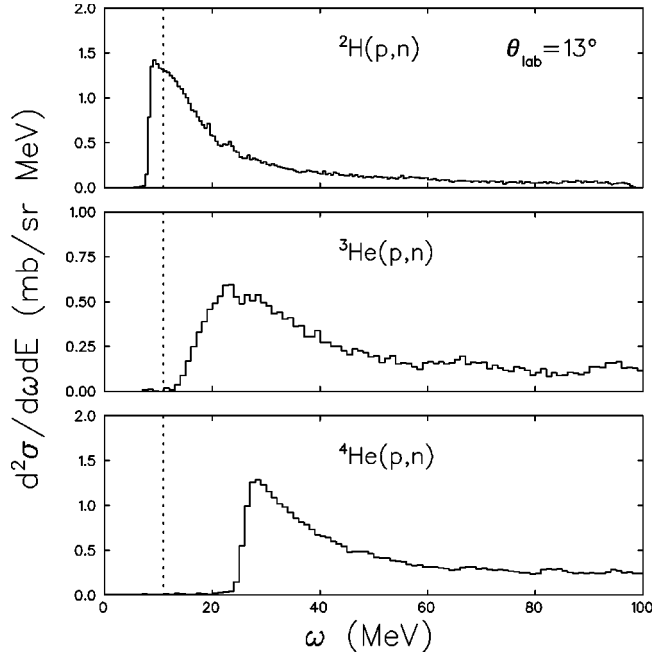

FIG. 7. Laboratory double differential cross section observed at $\theta_{\rm lab}=13°$ and $E_p=197$ MeV for the (p,n) reactions on ^{2}H and ^{3,4}He targets. The vertical dashed lines correspond to the energy loss for free np scattering.

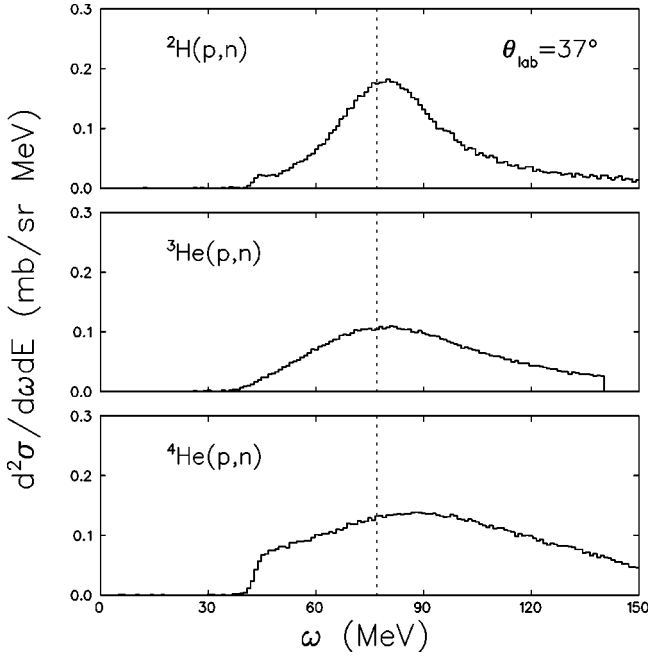

FIG. 8. Same as Fig. 7 but at $\theta_{\rm lab}=37°$.

there is only one neutron in ^{3}He versus two in ^{4}He. The present data (Table II) agrees with that observation. The sum cross section for the ^{2}H$(\vec{p},\vec{n})$ reaction and for the ^{3}He$(\vec{p},\vec{n})$ reaction at $q\approx 2.0$ fm^{-1} are approximately the same, reflecting the fact that in both cases there is only one neutron in the target nucleus. At $q\approx 0.9$ fm^{-1}, the sum cross section for the ^{2}H$(\vec{p},\vec{n})$ reaction is larger because it includes the cross section for the two-proton final-state interaction.

In Fig. 8 the double differential cross sections for the $(\vec{p},\vec{n})$ reaction on these targets at $\theta_{\rm lab}=37°$ and at $E_p=197$ MeV are shown. The dashed vertical lines represent the location of the energy loss for free np scattering. The quasielastic peak location for the ^{4}He(p,n) reaction is about 9 MeV higher than that for free np scattering, while for the (p,n) reactions on ^{2}H and ^{3}He the quasielastic peak is a few MeV higher than that for free np scattering. The spectra for the ^{4}He(p,n) reaction show a steep rise near threshold, indicating contributions from nuclear excitation in ^{4}Li [23].

TABLE II. Differential cross sections for (p,n) reactions on ^{2}H, ^{3,4}He at 197 MeV, in mb/sr as a function of q obtained by integrating the spectra in a 70-MeV wide region of excitation. The sum cross section has been obtained starting from threshold at $\theta_{\rm lab}=13°$ and centered around the quasifree peak at 37°. The free NN charge-exchange cross sections using the CD Bonn potential are also tabulated. An estimated 10% uncertainty is assigned to these values.

	$q\approx 0.8$ fm^{-1}	$q\approx 2.0$ fm^{-1}
	σ(mb/sr)	σ(mb/sr)
^{2}H	22.3	6.5
^{3}He	17.9	5.5
^{4}He	32.7	8.3
Free NN	28	7.4

2. Polarization-transfer coefficients for the ^{3,4}He$(\vec{p},\vec{n})$ reactions

Values for all D_{ij}, A_y, and P for ^{3}He (triangle data points) and ^{4}He (diamond data points) at $\theta_{\rm lab}=13°$ and 37° are presented in Figs. 9 and 10. The data have been binned in 10 or 15 MeV intervals depending on the statistics achieved at each angle. The statistics are best around the peak of the quasifree scattering cross section, which is the region with the largest double differential cross section. In this region typical uncertainties for the D_{ij} coefficients are about ± 0.05. The solid curves in all cases correspond to the Faddeev calculations done for the ^{2}H$(\vec{p},\vec{n})$ reaction at the corresponding angles. In general there is good agreement between the data and these calculations, which implies indirectly good agreement among the data sets for all three targets.

It is noted that values for P are different than those for A_y, being lower at $\theta_{\rm lab}=13°$ but higher at $\theta_{\rm lab}=37°$, pointing to other than two-body processes in these reactions. This was not the case at these angles for the ^{2}H$(\vec{p},\vec{n})$ reaction.

VI. DISCUSSION AND COMPARISON WITH CALCULATIONS

The empirical spin observables in quasielastic $(\vec{p},\vec{n})$ reactions obtained at 346 MeV [6] and 495 MeV [3] were transformed into spin-longitudinal and spin-transverse responses using the framework of a plane-wave impulse approximation with eikonal and optimal factorization approximations. These responses were compared to theoretical spin responses obtained with RPA calculations. The ratio of the empirical

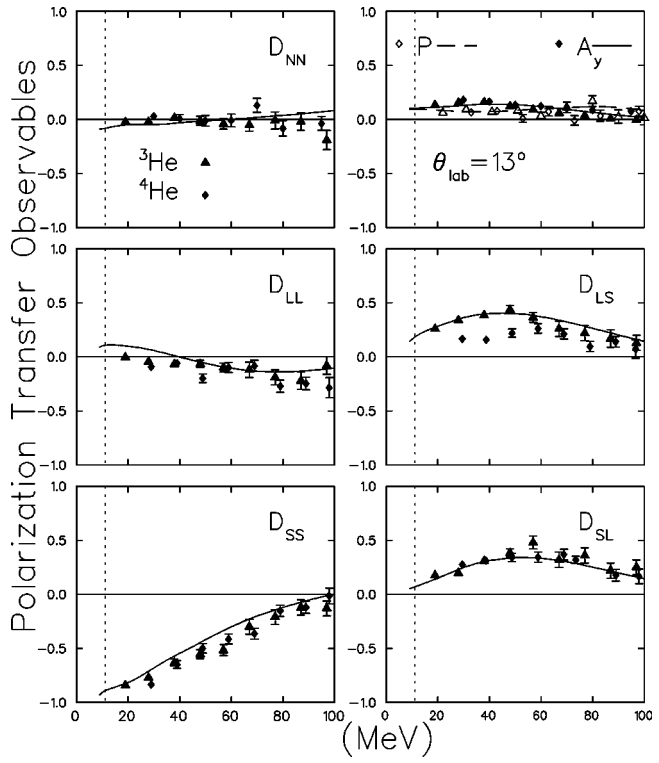

FIG. 9. Polarization-transfer coefficients, analyzing power, and induced polarization for the reactions $^{3,4}\mathrm{He}(\vec{p},\vec{n})$ measured at $E_p=197$ MeV and at $\theta_{\mathrm{lab}}=13°$, $q\approx 0.8$ fm^{-1}. The vertical dashed lines correspond to the energy loss for free np scattering. The solid lines are a result of optimal frame calculations using np values derived from the CD Bonn potential.

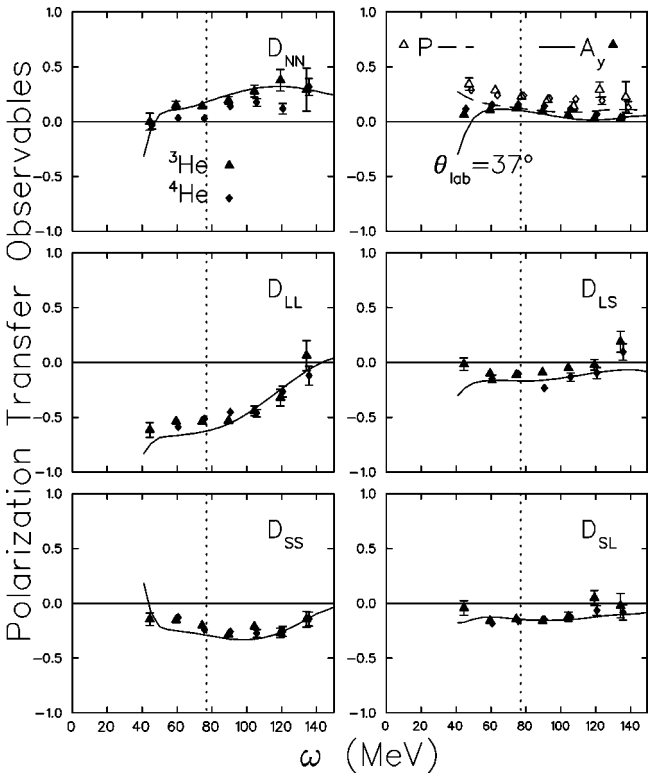

FIG. 10. Same as Fig. 9 but at $\theta_{\mathrm{lab}}=37°$, $q\approx 2.0$ fm^{-1}.

evaluated spin responses is close to 1.0, in contradiction with the expected spin-longitudinal enhancement due to pionic effects within the RPA framework. References [4,6] indicate a large excess in the observed spin-transverse response compared to the RPA calculations, which seems to mask the enhancement in the ratio of the responses, making them close to unity. See also Ref. [7].

We choose in this work to compare the spin observable results for the $^2\mathrm{H}(\vec{p},\vec{n})$ reaction *directly* with *ab initio* calculations, and results for the $^{3,4}\mathrm{He}(\vec{p},\vec{n})$ reaction with free np results using modern NN phase shift solutions. In the last few years a new generation of NN potentials, very well adjusted to NN data up to 300 MeV, has been constructed resulting in a $\chi^2\approx 1$ for all existing NN data. Among such potentials we find the Nijmegen93 [24], the AV18 [25], the CD Bonn [26], and the Arndt phase-shift analysis [27]. Sample calculations for Dij observables for the $^2\mathrm{H}(\vec{p},\vec{n})$ reaction at $E_p=200$ MeV and $\theta_{\mathrm{lab}}=37°$ are presented in Ref. [28]. Excellent agreement is observed for the D_{ij} values, independent of any of the above potentials or phase solutions used.

A. The optimal frame

In most calculations that describe nucleon-nucleus (NA) quasielastic collisions, the two-body amplitudes are derived from free on-shell amplitudes calculated from experimental phase shifts, assuming that the NN amplitudes depend only on the incident energy and the momentum transfer $\vec{q}$. In general these amplitudes should be evaluated off-shell, should include medium modifications, and should reflect the dependence on the momentum of the struck nucleon, which varies in NA systems due to its Fermi motion. In order to calculate quasielastic observables, it is necessary to integrate over the struck nucleon's Fermi momentum. This is greatly simplified if the two-body amplitudes are factored out of the integration by evaluating them in a frame where the struck nucleon's momentum has a constant ''optimal'' value. The ''optimal'' frame most appropriate for large-energy-loss quasifree scattering has been discussed in detail by Gurvitz [29], Smith [30], and Ichimura and Kawahigashi [31]. In Fig. 11, we present values obtained in the optimal frame for momentum transfer q, effective laboratory kinetic energy, and effective center-of-mass angle, as a function of energy loss ω calculated for the reaction $^2\mathrm{H}(p,n)$ at an incident energy of $E_{\mathrm{lab}}=200$ MeV. The solid lines, dashed lines, dot-dash lines, and dotted lines correspond to results obtained at $\theta_{\mathrm{lab}}=13°$, 24°, 37°, and 48°, respectively. The calculations at $\theta_{\mathrm{lab}}=13°$ and 24° are limited to an energy loss only up to $\omega=100$ MeV, which corresponds to the range of the present experiment. We note the large variation in the effective laboratory kinetic energy as a function of ω, especially for forward angles.

B. Faddeev calculations

Observables for the $^2\mathrm{H}(\vec{p},\vec{n})$ reaction may be calculated using exact solutions of $3N$ Faddeev equations with modern

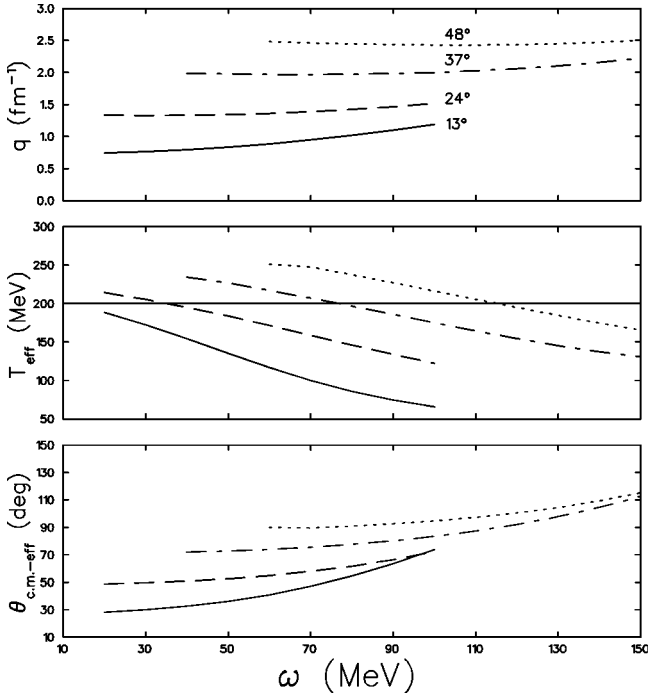

FIG. 11. Kinematic values calculated for the ^{2}H(p,n) reaction in the optimal frame at 200 MeV incident energy. Momentum transfer q, effective laboratory kinetic energy $T_{\rm eff}$, and effective c.m. angle $\theta_{\rm c.m.\ eff}$ are presented as a function of energy loss ω.

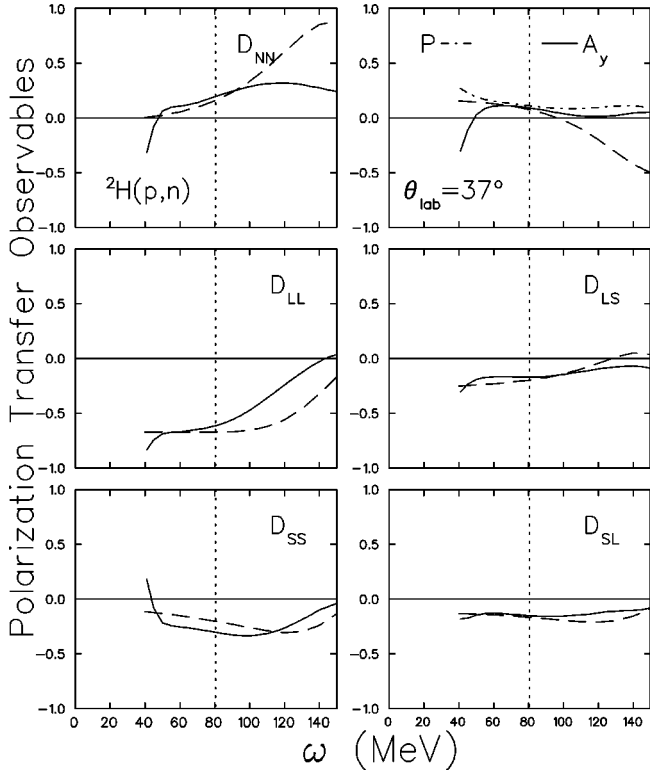

FIG. 12. Polarization-transfer coefficients, analyzing power, and induced polarization for the reaction ^{2}H$(\vec{p},\vec{n})$ calculated at 200 MeV incident energy and $\theta_{\rm lab}=37°$, using Faddeev equations with the CD Bonn potential (solid and dot-dashed lines) and optimal frame np values (dashed lines) obtained from the CD Bonn potential (see text). The vertical dashed lines correspond to the energy loss for free np scattering.

NN forces [32]. We have done such calculations using the CD Bonn [26] NN interaction. At a given energy, because of the short range nature of the NN force only a finite number of the total two-body angular momenta of the $2N$ system up to $j_{\rm max}$ and total angular momenta of the $3N$ system up to $J_{\rm max}$, contribute. At 200 MeV incident energy, converging results appear for $j_{\rm max}=5$ and $J_{\rm max}=25/2$. The Faddeev results (solid and dot-dashed curves) for spin polarization data at $\theta_{\rm lab}=37°$ are compared to the optimal frame np calculations with the CD Bonn [26] phase shift solutions (dashed curves) in Fig. 12. It is clear from the figure, that the agreement between both calculations is limited only to a narrow region of about ± 20 MeV around the quasielastic peak, represented by the vertical dotted lines. It is possible that at excitations above the quasielastic peak contributions from multiple scattering, not included in the optimal frame phase shift solutions, become important.

C. Polarization observables

We follow the procedure outlined by Ichimura and Kawahigashi [31], which uses relativistic transformations of observables to define four c.m.-frame polarization observables D_i in terms of the laboratory-frame polarization-transfer coefficients D_{ij}. These polarization observables are given by

$$D_o=(1/4)[1+D_{N'N}+(D_{S'S}+D_{L'L})\cos(\alpha_1) -(D_{S'L}-D_{L'S})\sin(\alpha_1)], \quad (4)$$

$$D_n=(1/4)[1+D_{N'N}-(D_{S'S}+D_{L'L})\cos(\alpha_1) +(D_{S'L}-D_{L'S})\sin(\alpha_1)], \quad (5)$$

$$D_q=(1/4)[1-D_{N'N}+(D_{S'S}-D_{L'L})\cos(\alpha_2) -(D_{S'L}+D_{L'S})\sin(\alpha_2)], \quad (6)$$

$$D_p=(1/4)[1-D_{N'N}-(D_{S'S}-D_{L'L})\cos(\alpha_2) +(D_{S'L}+D_{L'S})\sin(\alpha_2)], \quad (7)$$

with the constraint

$$D_o+D_n+D_q+D_p=1. \quad (8)$$

These observables follow from the original definitions of Bleszynski, Bleszynski, and Whitten [33] and are the spin independent D_o, the spin longitudinal D_q, and the two spin transverse D_n and D_p.

The laboratory-frame coordinates (S,N,L) and (S',N',L') were defined in Sec. II. The corresponding c.m. coordinates (q,n,p) are defined as $\mathbf{q}=(\mathbf{k}_f-\mathbf{k}_i)/(|\mathbf{k}_f-\mathbf{k}_i|)$, $\mathbf{n}=(\mathbf{k}_i\times\mathbf{k}_f)/(|\mathbf{k}_i\times\mathbf{k}_f|)$, and $\mathbf{p}=\mathbf{q}\times\mathbf{n}$, where k_i and k_f are the initial and final projectile momenta in the NA c.m. frame. The angles α_1 and α_2 are defined by

$$\alpha_1=\theta_{\rm c.m.}-\alpha_0, \quad (9)$$

$$\alpha_2=2\theta_p-\theta_{\rm c.m.}+\alpha_0, \quad (10)$$

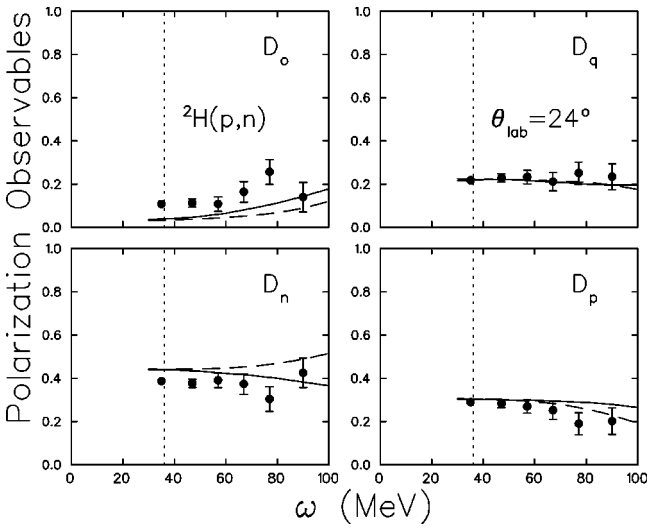

FIG. 13. Polarization observables for the reaction $^2\mathrm{H}(\vec{p},\vec{n})$ at $E_p=197$ MeV and at $\theta_{\mathrm{lab}}=24°$, $q\approx1.4$ fm^{-1}, compared to results obtained from Faddeev calculations (solid lines)with the CD Bonn potential and optimal frame np values (dashed lines) using the CD Bonn potential. See text.

where

$$\cos(\alpha_0)=\cos(\theta_{\mathrm{c.m.}})\cos(\theta_{\mathrm{lab}})+\gamma\sin(\theta_{\mathrm{c.m.}})\sin(\theta_{\mathrm{lab}}). \tag{11}$$

The angle α_0 is related to the relativistic angle Ω used by Ichimura and Kawahigashi [31] by $\alpha_0=\theta_{\mathrm{c.m.}}-\theta_{\mathrm{lab}}-\Omega$. The angle θ_p represents the angle between the incident beam direction and the vector **p** defined above.

The calculated c.m. polarization observables D_i are plotted in Figs. 13 and 14 at angles $\theta_{\mathrm{lab}}=24°$ and 37°, respectively, as a function of energy loss ω. The D_i values for the $^2\mathrm{H}(p,n)$ reaction are compared in Fig. 13 with results that

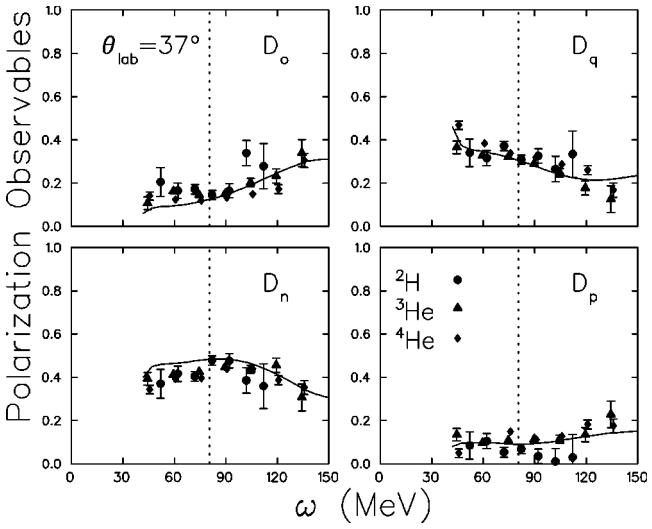

FIG. 14. Polarization observables for the reactions $^2\mathrm{H}(\vec{p},\vec{n})$, $^{3,4}\mathrm{He}(\vec{p},\vec{n})$ at $E_p=197$ MeV and at $\theta_{\mathrm{lab}}=37°$ ($q\approx2.0$ fm^{-1}) compared to results (solid lines) obtained from Faddeev calculations for the $^2\mathrm{H}(\vec{p},\vec{n})$ reaction. See text.

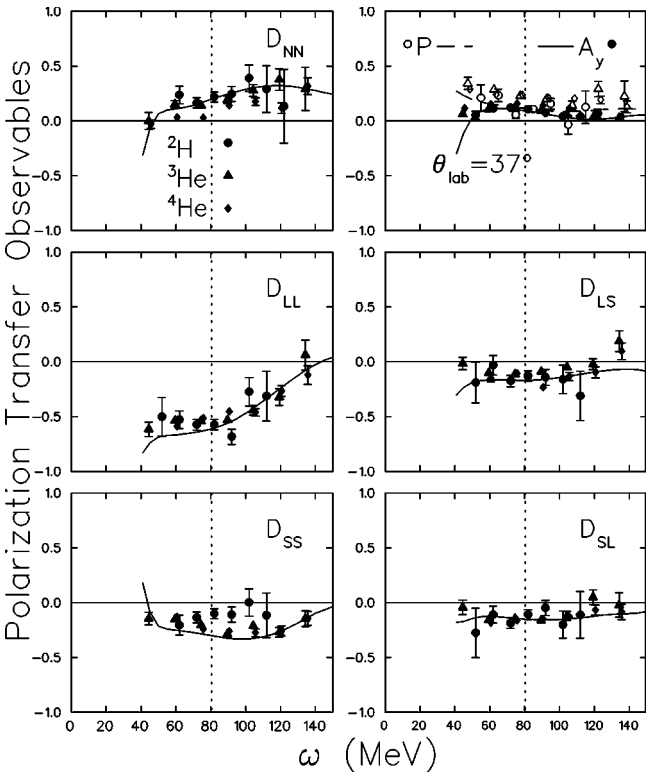

FIG. 15. Polarization-transfer coefficients, analyzing power, and induced polarization for quasielastic $(\vec{p},\vec{n})$ reactions on ^{2}H, ^{3,4}He targets at a scattering angle of $\theta_{\mathrm{lab}}=37°$, $q\approx2.0$ fm^{-1}, and at 197 MeV incident energy. The vertical dashed lines correspond to the energy loss for free np scattering. The solid lines represent results from Faddeev calculations for the $^2\mathrm{H}(\vec{p},\vec{n})$ reaction.

use as input the Faddeev D_{ij} values (solid curves), and with results derived in the optimal frame using the free NN values from the CD Bonn potential (dashed lines). The two calculations compare well to each other in the vicinity of the energy loss for free np scattering, represented by the dotted vertical lines, as was the case for the respective D_{ij} values shown in Fig. 12. In general, the empirical data agree slightly better with the Faddeev calculations. This is also true for data at the other two angles $\theta_{\mathrm{lab}}=13°$ and 48°, not shown here [22].

In Fig. 14 we compare D_i results at $\theta_{\mathrm{lab}}=37°$ obtained for the (p,n) reactions on all three targets ^{2}H and ^{3,4}He. The solid curves represent values obtained from the Faddeev-type of calculations for the $^2\mathrm{H}(p,n)$ reaction. Results for all three targets seem to cluster around the solid curves.

VII. SUMMARY

We have reported on a complete set of polarization-transfer coefficients measured at 197 MeV in the quasifree region for the $(\vec{p},\vec{n})$ reactions on ^{2}H and ^{3,4}He targets in the momentum-transfer range $q=0.75$–2.4 fm^{-1}. Data obtained on all these targets at $\theta_{\mathrm{lab}}=37°$ ($q\approx2.0$ fm^{-1}) are shown in Fig. 15. The figure seems to indicate that the D_{ij} values are, within statistics, not substantially different from each other, but a given D_{ij} is the same for all nuclei. The

resulting c.m. polarization observables D_i, as shown in Fig. 14 are subsequently also similar. The empirical results for the $^2\mathrm{H}(\vec{p},\vec{n})$ reaction are in good agreement with Faddeev-type calculations using the CD Bonn *NN* interaction. At this scattering angle $\theta_{\mathrm{lab}}=37°$, which corresponds to a momentum transfer $q\approx 2.0\ \mathrm{fm}^{-1}$, the $\pi+\rho+g'$ model of the spin-isospin dependent residual interaction predicts an enhancement of the spin-longitudinal response relative to the spin-transverse response, assuming a value $g'\approx 0.6$. This enhancement is attributed to nuclear-medium effects non existent in ^{2}H, but that should be strong in ^{4}He since this nucleus is very close to full nuclear density. The fact that the data for all these three nuclei are so similar indicates that the predicted enhancement in the ratio of the spin responses is not observed in these targets in the range of energy loss up to 150 MeV studied here.

ACKNOWLEDGMENTS

The authors would like to thank the careful work done by Bill Lozowski in preparing the targets used in these runs, and also the crew of the IUCF Cyclotron for their patience in preparing the incident beams in the proper polarization states. This study was supported in part by the National Science Foundation under Grants No. PHY-9722538, PHY-9803859, PHY-9409265, and PHY-9602872. One of the authors (H.W.) would like to thank the Polish Committee for Scientific Research under Grant No. 2P03B02818. The numerical calculations using the Faddeev formalism were done on the Cray T90 and on the Cray T3E of the NIC in Jülich, Germany. One of the authors (D.P.) would like to thank Junmei and Eric Hu for their support during the completion of this work.

[1] T. Ericson and W. Weise, in *Pions and Nuclei* (Oxford University Press, New York, 1988).
[2] W.M. Alberico, M. Ericson, and A. Molinari, Nucl. Phys. **A379**, 429 (1982).
[3] X.Y. Chen, T.N. Taddeucci, J.B. McClelland, T.A. Carey, R.C. Byrd, L.J. Rybarcyk, W.C. Sailor, D.J. Mercer, D.L. Prout, S. DeLucia, B. Luther, D.G. Marchlenski, E. Sugarbaker, J. Rapaport, E. Gulmez, C.A. Whitten, Jr., C.D. Goodman, W. Huang, Y. Wang, and W.P. Alford, Phys. Rev. C **47**, 2159 (1993).
[4] T.N. Taddeucci, B.A. Luther, L.J. Rybarcyk, R.C. Byrd, J.B. McClelland, D.L. Prout, S. DeLucia, D.A. Cooper, D.G. Marchlenski, E. Sugarbaker, B.K. Park, T. Sams, C.D. Goodman, J. Rapaport, M. Ichimura, and K. Kawahigashi, Phys. Rev. Lett. **73**, 3516 (1994).
[5] M. Ichimura and K. Kawahigashi, Phys. Rev. C **45**, 1822 (1992); **46**, 2117(E) (1992).
[6] T. Wakasa *et al.*, Phys. Rev. C **59**, 3177 (1999).
[7] K. Kawahigashi, K. Nishida, A. Itabashi, and M. Ichimura, Phys. Rev. C **63**, 044609 (2001).
[8] V.R. Pandharipande, J. Carlson, S.C. Pieper, R.B. Wiringa, and R. Schiavilla, Phys. Rev. C **49**, 789 (1994).
[9] V.R. Pandharipande, Nucl. Phys. **A577**, 131c (1994).
[10] D.S. Koltun, Phys. Rev. C **57**, 1210 (1998).
[11] C. Hautala *et al.*, following article, Phys. Rev. C **65**, 034612 (2000).
[12] M. Palarczyk *et al.*, Nucl. Instrum. Methods Phys. Res. A **457**, 309 (2001).
[13] J.W. Watson *et al.*, in *High Energy Spin Physics*, edited by Kenneth J. Heller and Sandra L. Smith, AIP Conf. Proc. No. 343 (AIP, Woodbury, NY, 1995), p. 203.
[14] C. M. Edwards, Ph.D. thesis, University of Minnesota, 1996.
[15] V. Derenchuck *et al.*, in *Proceedings from the 13th Internattional Conference on Cyclotrons and Their Applications* (World Scientific, Vancouver, Canada, 1995).
[16] S.P. Wells *et al.*, Nucl. Instrum. Methods Phys. Res. A **235**, 205 (1992).
[17] T.N. Taddeucci *et al.*, Phys. Rev. C **41**, 2548 (1990).
[18] L. Wang, Institute of Nuclear and Particle Physics Internal Report No. INPP-93-04, Ohio University, 1993.
[19] L. Wang *et al.*, Phys. Rev. C **50**, 2438 (1994).
[20] D. A. Cooper, Ph. D. thesis, The Ohio State University, 1997.
[21] G. Savopulos, Ph. D. thesish, Indiana University, 1998.
[22] C. L. Hautala, Ph. D. thesis, Ohio University, 1998.
[23] M. Palarczyk *et al.*, Phys. Rev. C **58**, 645 (1998).
[24] V.G.J. Stoks *et al.*, Phys. Rev. C **49**, 2950 (1994).
[25] V.R.B. Wiringa *et al.*, Phys. Rev. C **51**, 38 (1995).
[26] R. Machleidt *et al.*, Phys. Rev. C **53**, R1483 (1996).
[27] R.A. Arndt *et al.*, Phys. Rev. D **45**, 3995 (1992).
[28] J. Rapaport, in *Nuclear Responses and Medium Effects*, edited by T. Noro, H. Sakaguchi, H. Sakai, and T. Wakasa (Universal Academy Press, Tokyo, 1999), p. 52.
[29] S.A. Gurvitz, Phys. Rev. C **33**, 422 (1986).
[30] R. D. Smith, in *Proceedings of the International Conference on Spin Observables of Nuclear Probes*, Teluride, Colorado, 1988, edited by C. J. Horowitz, C. D. Goodman, and G. Walker (Plenum, New York, 1989), p. 15.
[31] M. Ichimura and K. Kawahigashi, Phys. Rev. C **45**, 1822 (1992); **46**, 2117(E) (1992).
[32] W. Gloeckle, H. Witala, D. Huber, H. Kamada, and J. Golak, Phys. Rep. **274**, 107 (1996).
[33] E. Bleszynski, M. Bleszynski, and C.A. Whitten, Jr., Phys. Rev. C **26**, 2063 (1982).